J. Fluid Mech. (2002), *vol.* 452, *pp.* 163–187.
DOI: 10.1017/S0022112001006784 Printed in the United Kingdom

Electrohydrodynamic stability: Taylor–Melcher theory for a liquid bridge suspended in a dielectric gas

By C. L. BURCHAM† AND D. A. SAVILLE

Department of Chemical Engineering, Princeton University, Princeton NJ 08544, USA

(Received 4 December 2000 and in revised form 1 August 2001)

A liquid bridge is a column of liquid, pinned at each end. Here we analyse the stability of a bridge pinned between planar electrodes held at different potentials and surrounded by a non-conducting, dielectric gas. In the absence of electric fields, surface tension destabilizes bridges with aspect ratios (length/diameter) greater than π. Here we describe how electrical forces counteract surface tension, using a linearized model. When the liquid is treated as an Ohmic conductor, the specific conductivity level is irrelevant and only the dielectric properties of the bridge and the surrounding gas are involved. Fourier series and a biharmonic, biorthogonal set of Papkovich–Fadle functions are used to formulate an eigenvalue problem. Numerical solutions disclose that the most unstable axisymmetric deformation is antisymmetric with respect to the bridge's midplane. It is shown that whilst a bridge whose length exceeds its circumference may be unstable, a sufficiently strong axial field provides stability if the dielectric constant of the bridge exceeds that of the surrounding fluid. Conversely, a field destabilizes a bridge whose dielectric constant is lower than that of its surroundings, even when its aspect ratio is less than π. Bridge behaviour is sensitive to the presence of conduction along the surface and much higher fields are required for stability when surface transport is present. The theoretical results are compared with experimental work (Burcham & Saville 2000) that demonstrated how a field stabilizes an otherwise unstable configuration. According to the experiments, the bridge undergoes two asymmetric transitions (cylinder-to-amphora and pinch-off) as the field is reduced. Agreement between theory and experiment for the field strength at the pinch-off transition is excellent, but less so for the change from cylinder to amphora. Using surface conductivity as an adjustable parameter brings theory and experiment into agreement.

1. Introduction

In his studies of charged jets and drops, Lord Rayleigh (1878, 1879*a*, *b*, 1882, 1891, 1892) introduced electrical forces into fluid dynamics by treating liquids as perfect conductors but until the 1960s most research focused on the behaviour of either perfect conductors or perfect dielectrics. To explain behaviour that was neither, Taylor (1966) modelled certain liquids as leaky dielectrics. Leaky dielectrics – usually homogeneous, apolar liquids with low electrical conductivities – allow free charge to congregate at interfaces where tangential electric stresses induce fluid motion. This

† Present address: Dow AgroSciences, L.L.C., Formulations Science and Technology, 9330 Zionsville Rd., Indianapolis, IN 46268, USA.

approach is known as the Taylor–Melcher theory to commemorate its originators (Melcher & Taylor 1969; Saville 1997). In this paper we employ the theory to describe the stability of a liquid bridge immersed in a dielectric gas.

Several earlier studies have dealt with the electrohydrodynamics of drops, jets, or liquid bridges. Taylor (1966) introduced the model to interpret drop deformation measurements in electric fields by Allan & Mason (1962) and demonstrated qualitative agreement between theory and experiment. Later, extensive experiments with isopycnic systems (Torza, Cox & Mason 1971) showed quantitative agreement with some systems and disagreement with others. Upon making special efforts to measure fluid properties, Vizika & Saville (1992) achieved reasonable agreement with Taylor's small-deformation theory. In cases where agreement was less satisfactory, small adjustments to the interfacial tension bring theory and experiment into close correspondence. Work by Tsukada *et al.* (1993) utilized a finite element technique to calculate drop deformations in steady fields with small inertial effects and their results also agree with the Vizika & Saville experiments. By treating nonlinear processes rigorously, Feng & Scott (1996) improved agreement between theory and experiment for higher field strengths and larger deformations. Surface transport – in this case convection of free charge – was shown to play a significant role by Feng (1999). It will turn out later that the stability of a bridge is acutely sensitive to another form of surface transport – Ohmic conduction along the surface layer.

Whereas the work on drops focuses on deformation, studies of jets or liquid filaments centre on stability. Experiments with jets are constrained by implementation difficulties, so most comparisons between theory and experiment are semi-quantitative. Nevertheless, analysis of a free liquid filament provides a basis for understanding the phenomena. First, a liquid filament becomes unstable due to surface tension when the deformation reduces the surface area, i.e. for an axisymmetric deformation whose wavelength exceeds the circumference. To stabilize this configuration, an axial electric field must provide the appropriate stresses. When the liquid behaves as a perfect dielectric, the electrical boundary condition at the interface ensures that the free charge is zero, i.e. the product of the dielectric constant and the normal component of the electric field is continuous across the interface. Thus, electrical stresses due to small deformations of a cylindrical filament in an axial field are always normal to the interface and proportional to $(\varepsilon_i - \varepsilon_e)^2(-\zeta)E_o^2\boldsymbol{n}$. Here, ε_i and ε_e represent dielectric constants of the filament and surroundings, ζ is the (signed) deformation relative to a circular cylinder, E_o^2 is the square of the applied field strength, and $\boldsymbol{n}$ is the outward-pointing normal. So, normal stresses due to polarization of the interface always tend to smooth perturbations. With a leaky dielectric immersed in a perfect dielectric the situation is more involved since free charge moves to the interface to modify the field and make the normal component of current vanish at the interface. Here the electric stress has components in the normal and tangential directions. The normal stress, now modified by the presence of free charge, is proportional to $(\varepsilon_i - \varepsilon_e)(-\zeta)E_o^2\boldsymbol{n}$ (Saville 1997). So, the sense of the normal force depends on the relative magnitudes of the dielectric constants. As suggested by the expression for the normal stress and confirmed by experiments, it is not possible to stabilize a leaky dielectric when its dielectric constant is less than that of the surrounding fluid (Sankaran & Saville 1993). Of course the magnitude of the field necessary for stability is complicated by a tangential stress, proportional to the product of the induced charge and the tangential field. Although Saville (1971) found qualitative agreement with Taylor's (1969) experiments on a water jet, a liquid bridge provides a more tractable system.

The liquid bridge configuration lends itself to studies of electric field effects since the contact lines are pinned. In his classic work, Plateau (1863, 1864, 1865, 1866) showed that a neutrally buoyant cylindrical bridge was stable, provided its length did not exceed its circumference. Raco (1968) was the first to stabilize a liquid bridge between electrodes in air by pulling a filament from a pool of liquid while increasing the potential of one plate. González *et al.* (1989) solved the *electrohydrostatic* equations to investigate the stability of a perfect dielectric bridge in an axial electric field. As expected, non-axisymmetric deformations are always stable and axisymmetric deformations above the Plateau limit can be stabilized with a sufficiently large field. Stability depends on three parameters: the aspect ratio, $\beta \equiv l/2a$ – the length of the bridge divided by its diameter; $S \equiv \varepsilon_e/\varepsilon_i$ – the ratio of the dielectric constant of the outer fluid to that of the inner fluid; and $\Delta \equiv a\varepsilon_i\varepsilon_o E_o^2/\gamma$ – the ratio of electric stresses to interfacial tension forces. Here, a is the radius of the bridge, ε_o is the permittivity of free space, and γ represents the interfacial tension. As expected, the theory shows that the size of the field required for stability increases as the dielectric 'contrast' decreases, i.e. as $S \to 1$. González *et al.* conducted experiments with an almost neutrally buoyant system – castor oil in a silicone oil bath – using an AC field to nullify charge transport and produce perfect dielectric behaviour. Their data agreed with the theory for $\beta > 4$; disagreements for $\beta < 4$ were attributed to buoyancy since the Bond number, $Bo \equiv g\Delta\rho a^2/\gamma$, was not zero. Here g represents the gravitational acceleration and $\Delta\rho$ is the density difference between the bridge and surrounding fluid. Later work at a Bond number of $O(10^{-2})$ showed better agreement with an amended theory (González & Castellanos 1993). Ramos, Gonzáles & Castellanos (1994) found good agreement when experimental data were compared to a theory that includes buoyancy.

Only two sets of experiments have been reported on leaky dielectric bridges. Sankaran & Saville (1993) used a mixture of castor oil and eugenol to form a neutrally buoyant liquid bridge in silicone oil. For aspect ratios above π, two distinct shape transitions were identified. Above a certain field strength, the bridge was a 'perfect' cylinder. Upon lowering the field strength, a cylinder-to-amphora shape transition was observed; at a specific (lower) field strength the bridge 'pinched-off' (asymmetrically) into separate drops. Interestingly, when the fluids were interchanged, an axial field destabilized the bridge for aspect ratios less than π, as predicted by the leaky dielectric model (Saville 1970). Sankaran & Saville also noted that the bridge always deforms with the 'bulge' nearest the positive electrode, indicating an unexplained electrical bias. No theory exists for two-phase, leaky dielectric bridges.

Burcham & Saville (2000) studied liquid bridges suspended in a dielectric gas, sulphur hexafluoride (SF_6). To minimize buoyancy, their experiments were carried out in a microgravity environment aboard the space shuttle *Columbia*. Because the fluid surrounding the liquid bridge was a dielectric gas, interphase charge transport was absent. Accordingly, as long as the bridge behaves as a leaky dielectric and charge relaxation is rapid, the precise level of conductivity is unimportant. This arrangement partially nullifies effects due to uncertainties in the conductivity, especially those due to moisture. However, it accentuates other charge transport mechanisms, e.g. surface conduction, should they be present. In steady fields, Burcham & Saville found transitions similar to those identified in liquid–liquid systems by Sankaran & Saville (1993). The purpose of the current work is to provide a theory of the behaviour of a leaky dielectric bridge in a gas.

Modelling the behaviour of liquid bridge in a dielectric gas is much less complicated than for a liquid–liquid system since the hydrodynamics of the outer phase can be

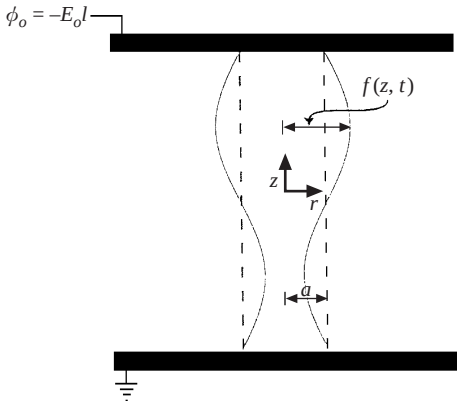

FIGURE 1. Sketch of a liquid bridge of length l. The undeformed bridge of radius a is indicated by dashed lines; solid lines indicate the deformed interface, $r = f(z, t)$.

ignored. Moreover, this configuration is particularly amenable to linear stability analysis since, in the undeformed base state, the electric field lines are parallel to the interface and the bridge is quiescent.

The paper is organized as follows. In § 2 a theory for analysing the stability of a leaky dielectric bridge is set out. Since interest centres on the demarcation between stability and instability, a linearized model is used in § 3 to formulate an eigenvalue problem that is solved numerically. Symmetric and antisymmetric deformations are studied and the results set out in § 4. As a consistency check, the special case of a perfect dielectric bridge is analysed using the formalism developed for the leaky dielectric. The agreement with the theory of González *et al.* (1989) is perfect. For a leaky dielectric bridge, antisymmetric deformations turn out to be the most unstable. The structure of the perturbation fields is also discussed, with particular attention to the flow caused by free charge induced on the interface. Section 5 is devoted to an extension of the Taylor–Melcher model to account for the effects of a surface conduction. Accordingly, the conductivity is anisotropic near the surface and current flowing into the surface from the bulk is transported laterally along the surface. Since this diminishes the local surface charge density, higher field strengths are required for stability. Comparisons with experiments by Burcham & Saville (2000) are discussed in § 6. The agreement between theory and experiment for the ('infinitesimal') cylinder–amphora transition is not nearly as good as it is at pinch-off. However, the addition of a surface conductivity permits the theory to be brought into correspondence with the experiments. Concluding observations are given in § 7. The details of the manipulations needed to obtain the characteristic equation for stability are given in the Appendix.

2. Taylor–Melcher theory for a liquid bridge

The modelling of electrohydrodynamic phenomena involves the continuity and momentum equations from hydrodynamics and Maxwell's equations for the electrostatics. The Taylor–Melcher model can be derived in a straightforward fashion from a detailed set of balance laws that take account of bulk effects such as charge transport (Saville 1997). Hydrodynamics and electrostatics are coupled through the interfacial stresses, leading to a set of coupled partial differential equations. For present purposes we simply outline the essential features of the model.

Consider the situation depicted in figure 1 where a bridge of length l is pinned

between parallel electrodes. To establish an axial field, a voltage, ϕ_o, is applied to one electrode while the other is earthed. This defines a reference field strength as $E_o \equiv -\phi_o/l$. For a cylindrical bridge, the field lines are perpendicular to the electrodes (and parallel with the bridge). In accord with the Taylor–Melcher theory, the bridge liquid is treated as an Ohmic conductor so the electric potential and electric field follow from solutions of Laplace's equation

$$\nabla^2\phi = 0, \tag{1}$$

with the field strength defined by

$$-\nabla\phi = \boldsymbol{E}. \tag{2}$$

If we scale lengths on the undeformed bridge radius and transform the potential and field strength according to

$$r \to ar, \quad z \to az, \quad \phi \to E_o a\phi \quad \boldsymbol{E} \to E_o\boldsymbol{E} \tag{3}$$

the differential equation is unchanged. The boundary conditions are as follows.

Constant potentials at the electrodes:

$$\phi = 0 \quad \text{at} \quad z = -\beta \quad \text{and} \quad \phi = -2\beta \quad \text{at} \quad z = \beta. \tag{4}$$

Conservation of current crossing the bridge surface:

$$\boldsymbol{E}_i \cdot \boldsymbol{n} = R\boldsymbol{E}_e \cdot \boldsymbol{n}, \quad R \equiv \frac{\sigma_e}{\sigma_i}. \tag{5}$$

Here, σ represents the electrical conductivity and the subscripts i and e represent the interior and exterior fluids, respectively. It is also convenient to treat the gas surrounding the liquid bridge as a leaky dielectric insofar as the electrical problem is concerned. Accordingly, R denotes the conductivity of the surrounding fluid divided by that of the bridge fluid. With this representation, the solution of the leaky dielectric problem can be converted to that for a perfect dielectric bridge in a perfect dielectric gas by setting $R = S \equiv \varepsilon_e/\varepsilon_i$.

Continuity of the tangential fields at the interface $r = f(z, t)$:

$$\boldsymbol{E}_i \cdot \boldsymbol{t} = \boldsymbol{E}_e \cdot \boldsymbol{t}. \tag{6}$$

To describe the hydrodynamics, the time, velocity, pressure, and stress are transformed according to

$$t \to \frac{\rho_i a v_i}{\gamma} t, \quad \boldsymbol{u} \to \frac{\gamma}{\rho_i v_i}\boldsymbol{u}, \quad p \to \frac{\gamma}{a}p, \quad \boldsymbol{\sigma} \to \frac{\gamma}{a}\boldsymbol{\sigma}. \tag{7}$$

The new symbols denote the density, ρ_i, and kinematic viscosity, v_i, of the bridge fluid. Upon omitting the inertial terms in anticipation of the linearization to follow, the dimensionless equations of motion are

$$Re\frac{\partial \boldsymbol{u}}{\partial t} = -\nabla p + \nabla^2\boldsymbol{u}, \quad \nabla \cdot \boldsymbol{u} = 0, \tag{8}$$

with the Reynolds number defined as

$$Re \equiv \frac{\rho_i a \gamma}{\mu_i^2}. \tag{9}$$

μ_i denotes the shear viscosity of the bridge fluid. Note that dynamics are coupled to the electric field through the electric stresses on the deformed interface.

The boundary conditions are no-slip on the electrode surfaces and a balance of normal (including interfacial tension) and tangential stresses on the bridge interface. The stress tensors in the two phases are:

$$\left.\begin{aligned}\boldsymbol{\sigma}_i &= -p_i\boldsymbol{\delta} + [\nabla\boldsymbol{u}_i + \nabla\boldsymbol{u}_i^T] + \Delta[\boldsymbol{E}_i\boldsymbol{E}_i - \tfrac{1}{2}\boldsymbol{E}_i\cdot\boldsymbol{E}_i\boldsymbol{\delta}],\\ \boldsymbol{\sigma}_e &= -p_e\boldsymbol{\delta} + S\Delta[\boldsymbol{E}_e\boldsymbol{E}_e - \tfrac{1}{2}\boldsymbol{E}_e\cdot\boldsymbol{E}_e\boldsymbol{\delta}].\end{aligned}\right\} \tag{10}$$

The first part on the right of these expressions represents the pressure and viscous stresses in a Newtonian fluid; the second part is Maxwell's electric stress tensor. The dimensionless group Δ is the ratio of electrical stresses to those from interfacial tension, i.e.

$$\Delta \equiv \frac{a\varepsilon_i\varepsilon_o E_o^2}{\gamma}. \tag{11}$$

Moreover, because the interface deforms, the kinematic condition must hold and so

$$\frac{\partial f}{\partial t} = \boldsymbol{u}_i\cdot\boldsymbol{n}. \tag{12}$$

The position of the interface is also constrained by conservation of volume so

$$\int_{-\beta}^{\beta} f^2 \mathrm{d}z = 2\beta. \tag{13}$$

Finally, at the electrodes the interface is 'pinned' at the location of the undeformed radius so

$$r = 1 \quad \text{at} \quad z = \pm\beta. \tag{14}$$

3. Linear stability analysis

3.1. *The base state and perturbation fields*

To continue the development, a base state is introduced to describe the configuration of the undisturbed bridge. In dimensionless form this is

$$\phi^o = -z - \beta, \quad \boldsymbol{u}^o = \boldsymbol{0}, \quad f^o = 1. \tag{15}$$

So, the modified pressures inside and outside the bridge are constant and denoted as

$$p_i^o = -\Pi_i^o, \quad p_e^o = -\Pi_e^o. \tag{16}$$

The normal stress boundary condition shows that the constants are related as

$$\Pi_i^o - \tfrac{1}{2}\Delta + 1 = \Pi_e^o - \tfrac{1}{2}\Delta S. \tag{17}$$

With the base state known, the analysis continues by studying small perturbations of amplitude δ. Based on previous work with jets and bridges, attention focuses on axisymmetric deformations. Accordingly,

$$f(z,t) = f^o + \delta\tilde{f}(z)\exp(\omega t), \tag{18}$$

$$\phi(r,z,t) = \phi^o(z) + \delta\tilde{\phi}(r,z)\exp(\omega t), \tag{19}$$

$$p(r,z,t) = p^o + \delta\tilde{p}(r,z)\exp(\omega t), \tag{20}$$

$$\boldsymbol{u}(r,z,t) = \boldsymbol{0} + \delta\tilde{\boldsymbol{u}}(r,z)\exp(\omega t), \tag{21}$$

with the perturbed state represented by a tilde. The velocity components in the r-, θ-, and z-directions are denoted as $\tilde{u}(r,z), 0, \tilde{w}(r,z)$.

Since the stress tensor is

$$\boldsymbol{\sigma}(r,z,t) = \boldsymbol{\sigma}^o + \delta\tilde{\boldsymbol{\sigma}}(r,z)\exp(\omega t), \tag{22}$$

the linearized stress tensors written in terms of base and perturbed states are

$$\tilde{\boldsymbol{\sigma}}_i = -\tilde{p}_i\boldsymbol{\delta} + \left[\nabla\tilde{u} + \nabla\tilde{\boldsymbol{u}}^T\right]_i + \Delta[\boldsymbol{E}^o\tilde{\boldsymbol{E}} + \tilde{\boldsymbol{E}}\boldsymbol{E}^o - \tfrac{1}{2}[\boldsymbol{E}^o\cdot\tilde{\boldsymbol{E}} + \tilde{\boldsymbol{E}}\cdot\boldsymbol{E}^o]\boldsymbol{\delta}]_i \tag{23}$$

and

$$\tilde{\boldsymbol{\sigma}}_e = -\tilde{p}_e\boldsymbol{\delta} + \Delta\left[\boldsymbol{E}^o\tilde{\boldsymbol{E}} + \tilde{\boldsymbol{E}}\boldsymbol{E}^o - \tfrac{1}{2}[\boldsymbol{E}^o\cdot\tilde{\boldsymbol{E}} + \tilde{\boldsymbol{E}}\cdot\boldsymbol{E}^o]\boldsymbol{\delta}\right]_e. \tag{24}$$

For the fluids under consideration the Reynolds number is small (≈ 0.1) so we adopt a quasi-static approximation for the equation of motion. Accordingly, the equations describing the (linearized) perturbed state derived from (1)–(8) are

$$\nabla^2\tilde{\phi} = 0 \tag{25}$$

and

$$\boldsymbol{0} = -\nabla\tilde{p} + \nabla^2\tilde{\boldsymbol{u}}, \quad \nabla\cdot\tilde{\boldsymbol{u}} = 0. \tag{26}$$

The boundary conditions are:

(i) The no-slip condition, pinning of contact lines, and constant potential on the electrode:

$$\tilde{\boldsymbol{u}} = \boldsymbol{0}, \quad \tilde{\phi} = 0, \quad \tilde{f} = 0 \quad \text{at} \quad z = \pm\beta. \tag{27}$$

On the free surface of the bridge we have

(ii) the kinematic condition:

$$\omega\tilde{f}(z) = \tilde{u}(1,z); \tag{28}$$

(iii) the balance of normal stresses:

$$\delta\exp(\omega t)\left[(\tilde{\sigma}_{rr})_i - (\tilde{\sigma}_{rr})_e - 2\frac{\mathrm{d}\tilde{f}}{\mathrm{d}z}((\sigma^o_{rz})_i - (\sigma^o_{rz})_e) - \tilde{f} - \frac{\mathrm{d}^2\tilde{f}}{\mathrm{d}z^2}\right] + (\sigma^o_{rr})_i - (\sigma^o_{rr})_e + 1 = 0 \tag{29}$$

and tangential stresses:

$$\delta\exp(\omega t)\left[(\tilde{\sigma}_{zr})_i - (\tilde{\sigma}_{zr})_e + \frac{\mathrm{d}\tilde{f}}{\mathrm{d}z}\left((\sigma^o_{rr} - \sigma^o_{zz})_i - (\sigma^o_{rr} - \sigma^o_{zz})_e\right)\right] + (\sigma^o_{zr})_i - (\sigma^o_{zr})_e = 0; \tag{30}$$

(iv) the continuity of current:

$$\frac{\mathrm{d}\tilde{f}(z)}{\mathrm{d}z} + \left.\frac{\partial\tilde{\phi}_i(r,z)}{\partial r}\right|_{r=1} = R\frac{\mathrm{d}\tilde{f}(z)}{\mathrm{d}z} + R\left.\frac{\partial\tilde{\phi}_e(r,z)}{\partial r}\right|_{r=1}; \tag{31}$$

(v) the continuity of the tangential components of the electric field:

$$\tilde{\phi}_i(1,z) = \tilde{\phi}_e(1,z). \tag{32}$$

Finally, the bridge volume is conserved so

(vi)
$$\int_{-\beta}^{\beta}\tilde{f}(z)\,\mathrm{d}z = 0. \tag{33}$$

At this point the problem is defined and the coupled hydrodynamic and electrostatic problems can be solved. The potentials inside and outside the liquid bridge are

$$\tilde{\phi}_i(r,z) = -\sum_{k=0}^{\infty} A_k\frac{I_0(\alpha_k r)}{I_0(\alpha_k)}\sin(\alpha_k(z+\beta)), \tag{34}$$

$$\tilde{\phi}_e(r,z) = -\sum_{k=0}^{\infty} A_k \frac{K_0(\alpha_k r)}{K_0(\alpha_k)} \sin(\alpha_k(z+\beta)), \tag{35}$$

where $I_0(\alpha_k r)$ and $K_0(\alpha_k r)$ are the modified Bessel functions. The index k represents the number of half-waves between the electrodes, i.e.

$$\alpha_k = \frac{k\pi}{2\beta}. \tag{36}$$

The unknown coefficients, A_k, are related to the interface position through the equation for the continuity of current as

$$\frac{\mathrm{d}\tilde{f}(z)}{\mathrm{d}z}(R-1) + \sum_{k=1}^{\infty} \left(A_k \alpha_k \sin(\alpha_k(z+\beta)) \left(R\frac{K_1(\alpha_k)}{K_0(\alpha_k)} + \frac{I_1(\alpha_k)}{I_0(\alpha_k)} \right) \right) = 0. \tag{37}$$

However, the A_k cannot be determined until the position of the interface is established so the equations of motion must be solved.

The modified pressure and velocity fields are found by solving the equations of motion, (26), rewritten in terms of the stream function, ψ, defined as

$$\tilde{u}(r,z) = -\frac{1}{r}\frac{\partial \psi}{\phi z}, \quad \tilde{w}(r,z) = \frac{1}{r}\frac{\partial \psi}{\partial r}. \tag{38}$$

Then, upon taking the curl of the momentum equation we have

$$\mathrm{E}^2\mathrm{E}^2\psi = 0 \tag{39}$$

where

$$\mathrm{E}^2 \equiv \frac{\partial^2}{\partial r^2} - \frac{1}{r}\frac{\partial}{\partial r} + \frac{\partial^2}{\partial z^2}. \tag{40}$$

Using separation of variables, the stream function inside the bridge is written as

$$\psi(r,z) = \psi_R(r)\psi_Z(z). \tag{41}$$

However, as it turns out, Fourier series cannot readily be employed for the z-dependence since no harmonic function will satisfy the boundary conditions at the electrodes. Nicolás (1992) dealt with this problem using Papkovich–Fadle functions, a biharmonic, biorthogonal set of functions first used in elasticity problems by Smith (1952) and later by Joseph (1975, 1977), and Joseph & Sturges (1975, 1978). The Papkovich–Fadle (or P–F) functions can be separated into symmetric and antisymmetric functions of z and, when translated into the interface deformation, the symmetric P–F functions represent an odd number of 'half-waves' on the interface, namely an antisymmetric perturbation. The antisymmetric P–F functions yield a symmetric deformation with an even number of half-waves. Due to the conservation of volume, the minimum number of 'half-waves' on the interface is two. The behaviour of both types of deformation will be discussed in the next section. The details of the analysis of antisymmetric perturbations are described in the Appendix; Burcham (1998) explains the problem for symmetric deformations.

First we write the z-dependence of the potential in terms of antisymmetric and symmetric parts using a trigonometric identity

$$\sin(\alpha_k(z+\beta)) = \sin(\alpha_k z)\cos(\alpha_k \beta) + \cos(\alpha_k z)\sin(\alpha_k \beta). \tag{42}$$

Therefore, when k is odd the expression is even and this pertains to symmetric deformations; even k-values represent antisymmetric deformations.

The solution for either type of deformation proceeds by solving for the stream function, subject to the appropriate boundary conditions at the electrodes and on the interface. Next the modified pressure can be calculated from the r- and z-components of the equation of motion and the deformed interface shape function found from the normal stress balance, subject to the conservation of volume. Then, using the stream function to compute the modified pressure and interface position, the unknown coefficients can be determined using the tangential stress condition, the kinematic condition, and the electrical boundary conditions. Finally, an eigenvalue problem is solved to find the conditions for neutral stability. Further details are set out in the Appendix.

4. Stability of a liquid bridge in a dielectric gas

Solutions to the bridge stability problem depend parametrically on the field strength and interfacial tension as embodied in Δ, the aspect ratio β, the dielectric constant ratio S, and the conductivity ratio R. The expression for the deformation involves two infinite series, a Papkovich–Fadle series to describe the hydrodynamics and a Fourier series for electrostatics. When investigating neutral stability, the amplification parameter ω is set to zero so Δ is the eigenvalue in (A 45). Setting $\omega = 0$ is equivalent to assuming that 'exchange of stabilities' applies. Although we have not attempted to prove that ω is real at the point of neutral stability, a limited number of numerical experiments indicate that this is the case, cf. § 4.3. The coefficients in the series can be employed to represent the interface position, charge, stream function, and potential.

4.1. *Consistency with previous work*

Before examining the behaviour of a leaky dielectric bridge, it is important to check the formulation for convergence and consistency. First, the convergence of the P–F series is rapid. For antisymmetric or symmetric deformations, three terms give the growth rate for $\beta > \pi$ to within 1% with $\Delta = 0$; even better accuracy is obtained with $\Delta \neq 0$. The Fourier series also converge rapidly and expanding the solution beyond 12 terms changes the numerical results by less than 0.1%. Convergence does not appear to be influenced by the magnitude of S, but depends weakly on β. For most of the results reported here, three terms in the P–F series were used along with a 21-term Fourier series for antisymmetric modes or a 22-term series for the symmetric modes. Naturally, the results from the model agreed with Plateau's $\beta = \pi$ criterion for a neutrally stable bridge without an electric field. Comparisons were also made with amplification rates calculated for an unstable viscous bridge without an electric field (Nicolás 1992). The results are virtually identical.

Another consistency check involved comparison with the treatment of a perfect dielectric bridge by González *et al.* (1989). This necessitated a slight modification of the boundary condition on the electric field since, for a perfect dielectric, $\boldsymbol{E}_i \cdot \boldsymbol{n} = S\boldsymbol{E}_e \cdot \boldsymbol{n}$. With the current formulation this can be accomplished simply by setting $R = S$. The numerical values computed for the β–Δ relations are identical with those computed with the González *et al.* formulas.

To see the effect of pining the ends, results for a perfect dielectric bridge were compared with those for a perfect dielectric jet (Nayyar & Murty 1960). Recall the relation between wavenumber and β from (36), i.e. $\alpha_s = k\pi/2\beta$ where β is the wavelength of the disturbance divided by the diameter. Using this definition of α_s, the

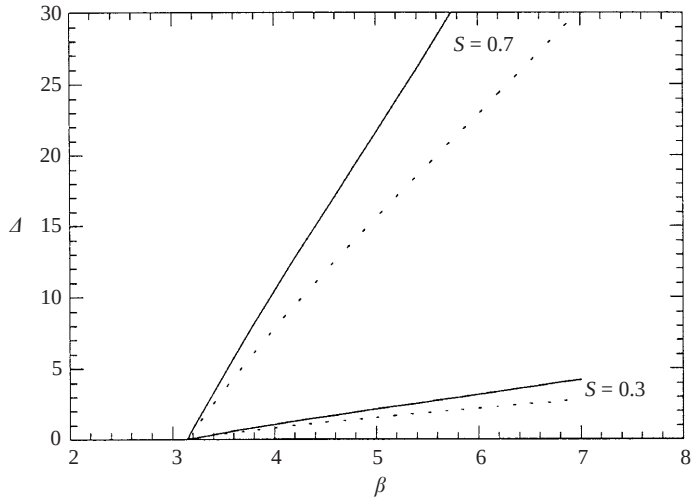

FIGURE 2. Neutral stability relations for a perfect dielectric bridge (——) and a jet (— — —) in a gas for the lowest antisymmetric deformation mode.

curve of neutral stability is given by

$$(\alpha_k^2 - 1) + \frac{\Delta(S-1)^2\alpha_k}{S(K_1(\alpha_k)/K_0(\alpha_k)) + I_1(\alpha_k)/I_0(\alpha_k)} = 0. \tag{43}$$

As mentioned earlier, the antisymmetric case corresponds to $k = 2$. β–Δ relation calculated from (43) is shown in figure 2 along with the results predicted using the perfect dielectric bridge model. The comparison shows that pinning the ends of the bridge increases the field required for stability.

4.2. *Neutral stability*

Having demonstrated that the computation procedure is consistent with previous results, we proceed to investigate the stability of a leaky dielectric bridge. Some neutral stability curves for a single-phase bridge are depicted in figure 3; figure 4 shows the neutral deformation interface shapes. Figure 3 also shows the stability relations extending into the region where $\Delta < 0$ to illustrate that the relations cross the $\Delta = 0$ axis with a positive slope. Nevertheless, $\Delta < 0$ is inaccessible since electrohydrodynamic phenomena are proportional to the square of the field strength. As illustrated on the figure, the first mode to become unstable at $\beta = \pi$ and $\Delta = 0$ corresponds to an antisymmetric deformation ($k = 2$) with two 'half-waves' on the interface (figure 4). The $k = 3$ mode, a symmetric deformation with three 'half-waves' on the interface, appears at $\beta \approx 4.5$. Both modes are unstable at $\beta = 5$ and $\Delta = 0$. As Δ is increased, the antisymmetric deformation is stabilized at $\Delta \approx 0.1$; the symmetric mode requires a larger field and so $\Delta \approx 0.37$ at neutral stability. Above this value the bridge is cylindrical. More modes become active as β is increased and at $\beta = 7$ two antisymmetric ($k = 2$ and 4) and one symmetric ($k = 3$) modes appear. The $k = 2$ mode is the most unstable in the sense that the highest field strength is required to suppress its growth.

Δ–β relations for the most unstable antisymmetric and symmetric modes are shown in figure 5 and figure 6 for various dielectric constant ratios. Comparing these results to those predicted for a perfect dielectric bridge discloses some qualitative similarities. As the dielectric constant contrast decreases ($S \to 1$), the electric field needed to

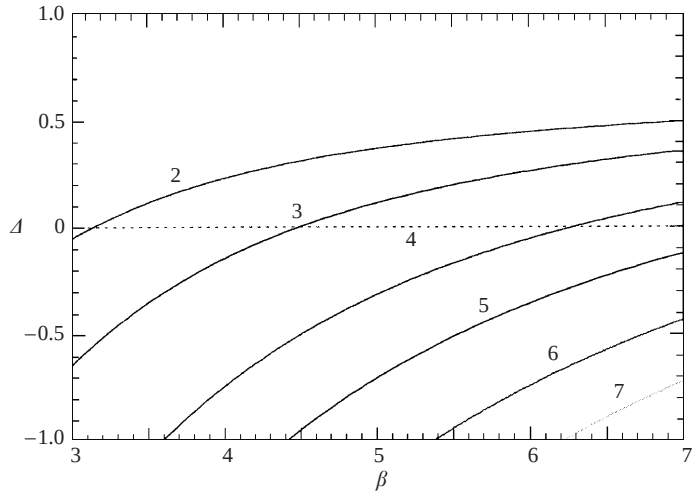

FIGURE 3. Neutral stability relations for different modes of deformation ($S = 0.215$, $R = 0$). The stable region lies above a specific curve. Even values of k (the number of 'half-waves' in the deformation) correspond to antisymmetric modes; odd values to symmetric modes. These values of S and R were chosen for consistency with conditions used in the experiments to be discussed.

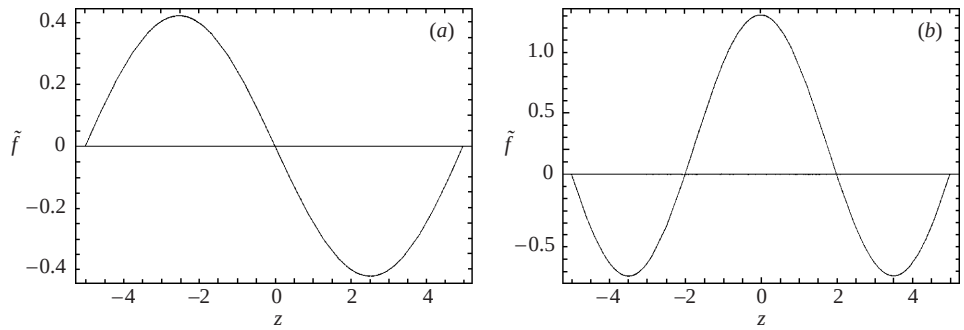

FIGURE 4. Neutrally stable interface shape perturbations, $\tilde{f}$, for $\beta = 5$ ($S = 0.215$, $R = 0$). Antisymmetric mode $k = 2$ (a); symmetric mode $k = 3$ (b).

stabilize the bridge increases since less free charge is induced at the interface. Also, with $\beta > \pi$ a bridge cannot be stabilized when $S = 1$, because no free charge can be induced and there are no polarization forces.

While results for leaky dielectric and perfect dielectric bridges are qualitatively similar (cf. figure 2 and figure 5) the electric field parameter necessary for stability with a leaky dielectric is much smaller. For example, with $\beta = 5$ and $S = 0.8$, Δ must be larger than 1.45 to ensure stability for a leaky dielectric liquid compared to $\Delta > 54.0$ with a perfect dielectric. The difference is due to free charge accumulation at the interface and the extra stress that enhances the effect of the field.

When $S > 1$, a striking change in behaviour is found compared to $S < 1$. For $S < 1$, the most unstable mode is the antisymmetric mode with two half-waves on the interface. However, when $S > 1$, the dielectric constant of the 'outer fluid' exceeds that of the bridge and the field necessary for neutral stability increases with the number of waves present on the interface (figure 7). Given the possibility of infinitesimal waves of every wavelength, it should be impossible to stabilize the bridge with an electric

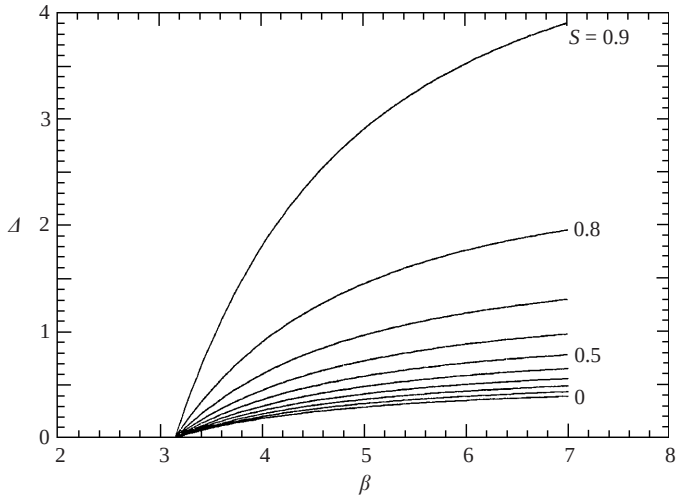

FIGURE 5. Neutral stability relations for the first antisymmetric mode for a leaky dielectric bridge ($S < 1$, $R = 0$).

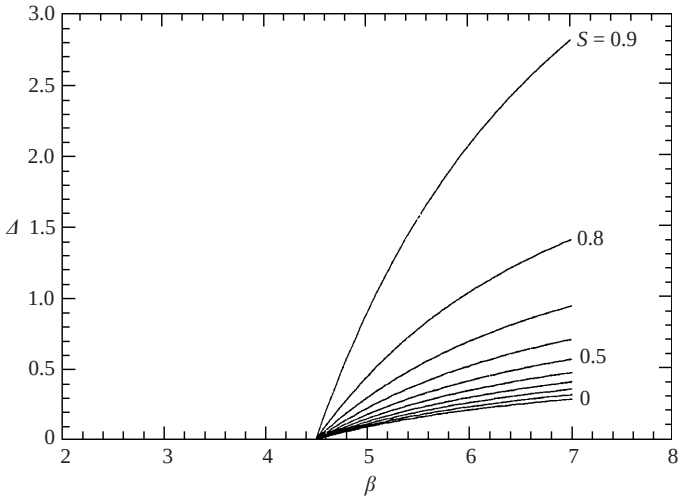

FIGURE 6. Neutral stability relations for the first symmetric mode for a leaky dielectric bridge ($S < 1$, $R = 0$).

field when $S > 1$. Moreover, an otherwise stable bridge ($\beta < \pi$) is destabilized by an axial field. Similar characteristics were found experimentally for isopycnic bridges (Sankaran & Saville 1993).

It is also interesting to examine the effects of conduction in the outer fluid, even when the hydrodynamics of the outer phase are ignored. Since conduction in the outer fluid allows charge to leak off the interface, the field required for neutral stability increases with R (figure 8). Similar behaviour is found when R is fixed while $S \to 1$, since this also reduces the charge at the interface.

4.3. *Structure of the perturbed fields*

Further insight into bridge behaviour follows by inspecting the perturbation fields. Figure 9 shows the perturbation potential, which is zero on the electrodes ($z = \pm\beta$),

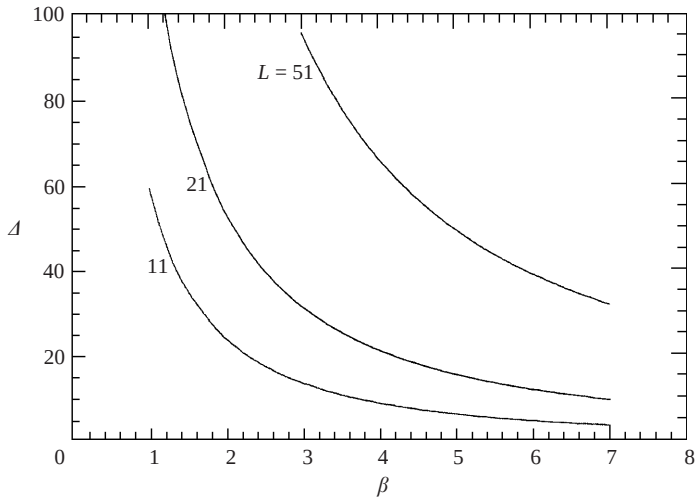

FIGURE 7. Neutral stability relations for a leaky dielectric bridge for $L = 11$, 21 and 51 half-waves ($S = 4.66$, $R = 0$). The unstable region lies below a particular curve.

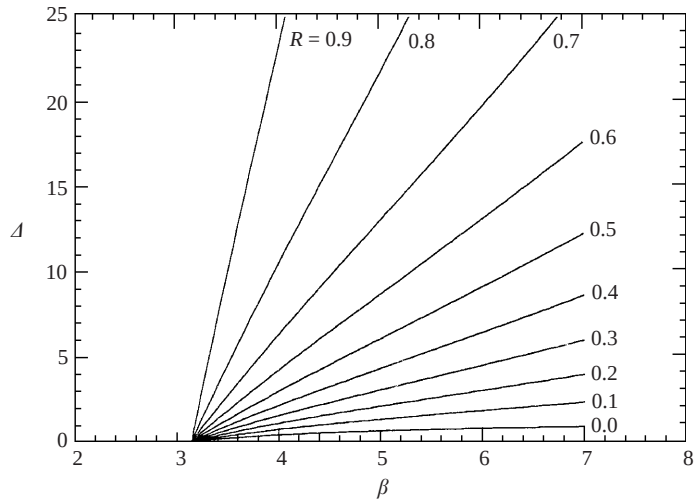

FIGURE 8. The effect of conduction in the outer fluid on the stability relations for the first antisymmetric mode with $S = 0.5$.

largest at the midplane ($r = 1, z = 0$), and decreases rapidly moving away from the bridge. Potentials inside and outside the bridge match at the deformed interface (bold line) as stipulated by the boundary conditions. From the perturbation potential, the perturbation charge induced on the interface can be calculated as

$$q = S\boldsymbol{E}_e \cdot \boldsymbol{n} - \boldsymbol{E}_i \cdot \boldsymbol{n} = \delta\tilde{q}(z)\exp(\omega t) \tag{44}$$

so

$$\tilde{q}(z) = (S\tilde{E}_{e,r}(1,z) - \tilde{E}_{i,r}(1,z)) + (1-S)\frac{\mathrm{d}\tilde{f}(z)}{\mathrm{d}z}. \tag{45}$$

The interfacial charge for the lowest antisymmetric mode (two half-waves) tracks, approximately, the 'slope' of the interface (figure 10). The charge on a deformed inter-

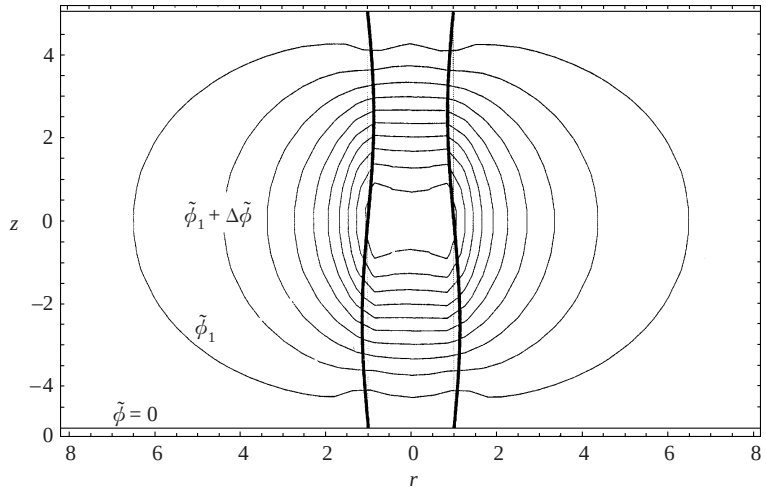

FIGURE 9. Equipotential lines ($\tilde{\phi}_1 = 0.1$ and $\Delta\tilde{\phi} = 0.165$) near a neutrally stable bridge ($\beta = 5$, $\Delta = 0.369$, $S = 0.215$).

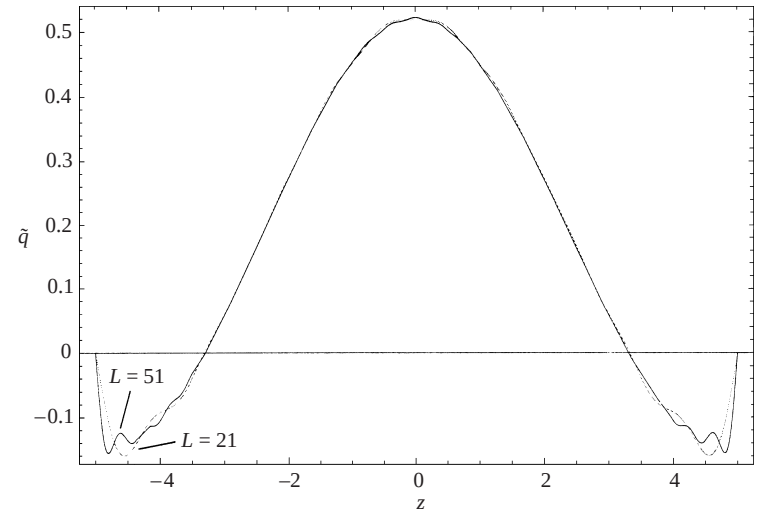

FIGURE 10. Interfacial charge for a deformed liquid bridge in the lowest antisymmetric mode at the point of neutral stability ($\beta = 5$, $\Delta = 0.369$, $S = 0.215$). L denotes the number of terms in the expansion. The effects of truncation are evident in the 'ripples' near the ends of the bridge.

face is depicted schematically on figure 11. The stabilizing effects of the electric charge arise from both the normal and tangential components of the electric stress. Since the normal stress is proportional to $(\varepsilon_i - \varepsilon_e)(-\zeta)\boldsymbol{E}_o^2\boldsymbol{n}$, it acts to 'level' perturbations. The tangential stress, which is proportional to the product of the induced charge and the axial field in the base state, forces the positively charged part of the interface away from the 'bulge'. Both effects reduce the deformation.

The streamlines are also interesting and the flow in a neutrally stable bridge in an axial field consists of a single toroidal recirculation (figure 12). Note the correspondence between the flow pattern and the tangential electric stress on the interface, cf. figure 11.

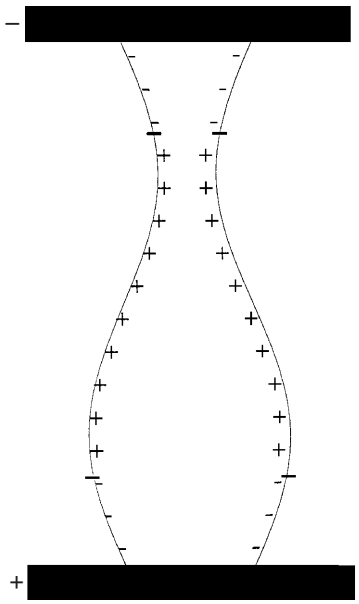

FIGURE 11. Schematic diagram of the charge on the interface of a liquid bridge ($\beta = 5$, $\Delta = 0.369$, $S = 0.215$). The 'ticks' denote rings where the charge is zero.

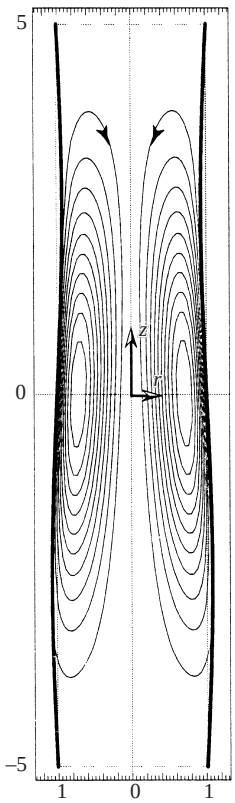

FIGURE 12. Streamlines and interface position for a neutrally stable liquid bridge ($\beta = 5$, $\Delta = 0.369$, $S = 0.215$); arrows indicate the direction of flow.

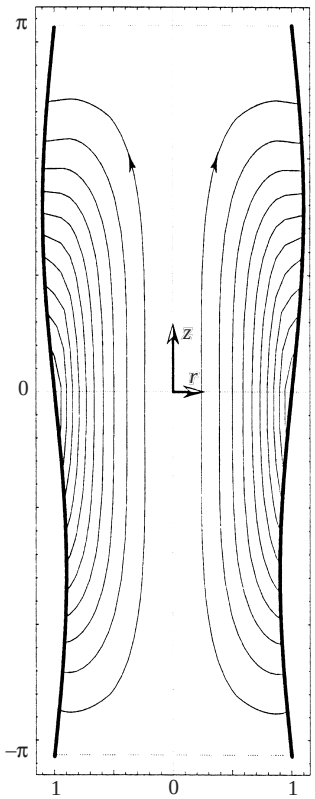

FIGURE 13. Streamlines and interface position for an unstable bridge with β slightly larger than π and $\Delta = 0$. Arrows indicate the direction of flow.

The behaviour of an unstable liquid bridge in the absence of a field is illustrated in figure 13. As expected, the deformation grows as liquid flows from the neck towards the bulge as interfacial tension pulls fluid out of the pinch. In an axial field with Δ slightly below the neutral stability value where the electrical stresses are unable to stabilize the bridge, the streamlines are similar to those in figure 13.

Finally, figure 14 depicts the ω–Δ relationship as the field is increased to stabilize a bridge. The field suppresses the growth rate dramatically at first and then levels out. Note that the growth rate is rather flat in the neighbourhood of the neutral stability point. The results shown on figure 14 were generated by solving for Δ with β and ω fixed. Finding ω given Δ and β is more challenging due to the behaviour of the determinant of the coefficient matrix, which changes rapidly near $\omega = 0$ in this format.

5. The leaky dielectric model with surface conduction

The leaky dielectric model with an isotropic bulk conductivity is the simplest representation of charge transport by dissolved ions. However, current flow, especially near an interface, is complicated by the formation of diffuse electrical double layers. Accordingly, the conductivity in the diffuse layer differs from that in the bulk. On a macroscopic scale, diffuse layer effects can be represented with a 'surface conductivity' (Russel, Saville & Schowalter 1991). Thus, while bulk conduction is isotropic, charge

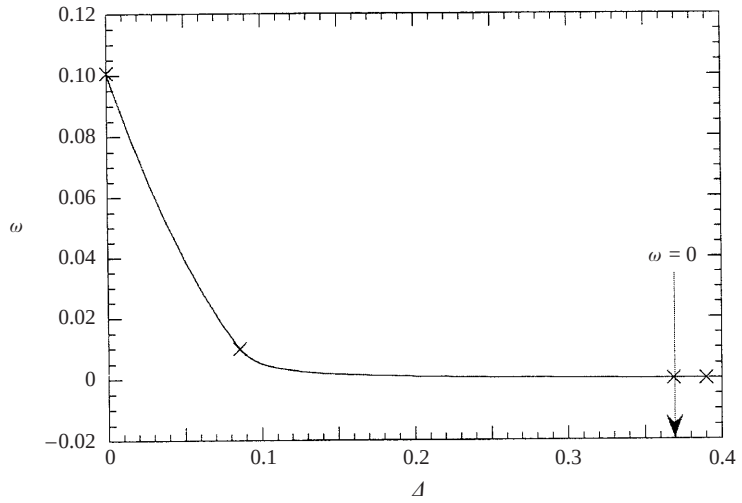

FIGURE 14. ω–Δ relation for $\beta = 5$ and $S = 0.215$.

transport near an interface is anisotropic since the flux into the interface can be balanced by lateral 'surface' conduction. To capture this effect with a perfect dielectric outer phase, 'lateral surface transport' can be added to the boundary conditions as an Ohmic process. Using σ_s to denote a surface conductivity modifies the charge transport boundary condition to (in dimensionless form)

$$\boldsymbol{E}_i \cdot \boldsymbol{n} = R\boldsymbol{E}_e \cdot \boldsymbol{n} + R_s \nabla_s \cdot \boldsymbol{E}_i, \tag{46}$$

where ∇_s is the dimensionless surface divergence and R_s is the *surface* conductivity ratio defined as

$$R_s \equiv \frac{\sigma_s}{a\sigma_i}. \tag{47}$$

This modifies the charge conservation boundary condition and changes (A 25) to

$$(R-1)Z_l b + A_l \beta(S_l + R_s \alpha_l^2) + \omega(R-1) \sum_{m=-\infty}^{\infty} B_m D_m P_{lm} + \omega(R-1) \sum_{m=-\infty}^{\infty} B_m C_m Q_{lm} = 0 \tag{48}$$

for an antisymmetric deformation. Neutral stability curves calculated for a castor oil bridge using the new system of equations are shown in figure 15. As expected, inclusion of surface transport destabilizes the bridge by providing a pathway for charge redistribution on the interface.

6. Comparisons between theory and experiment

Theoretical results are compared with experimental data (Burcham & Saville 2000) in figure 16. As expected, cylindrical bridges formed in a dielectric gas at aspect ratios below the Plateau value were stable. Using a high field strength, cylindrical bridges with $\beta > \pi$ could be formed. Then, upon lowering the field two transitions were identified: first, an antisymmetric change from a circular cylinder to an amphora shape followed, at a lower field, by pinch-off into two drops. Although both transitions follow trends predicted by the Taylor–Melcher model, they occur at Δ-values higher than predicted by the model. The correspondence between the pinch-off field and the leaky dielectric model is unexpected since the theory is based on small deformations.

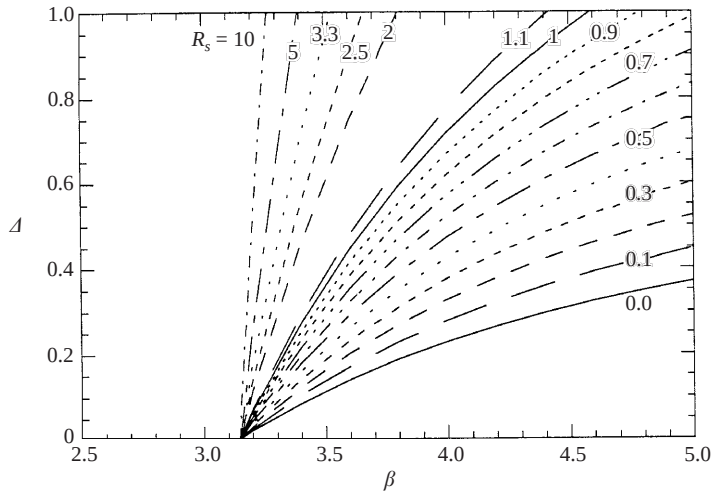

FIGURE 15. The effects of surface conductivity, R_s, on neutral stability relations for a castor oil bridge in a dielectric gas ($R = 0$, $S = 0.215$).

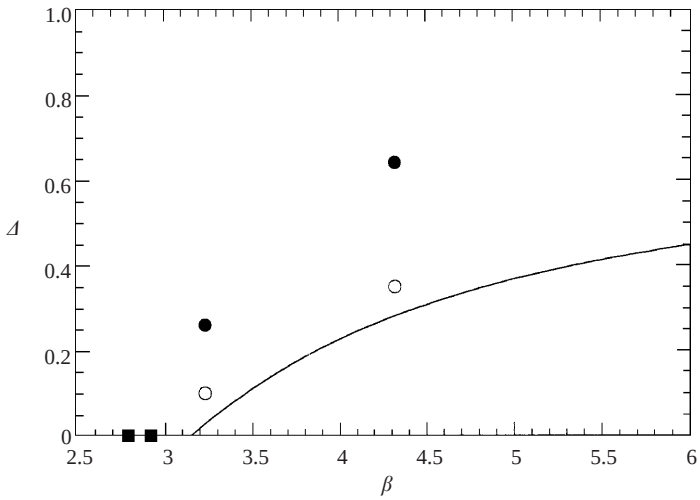

FIGURE 16. Comparison of experimental results (symbols) for a castor oil bridge in a dielectric gas to predictions from the leaky dielectric model for the first antisymmetric mode, $S = 0.21$ and $R = 0$. For $\beta < \pi$, ■ denotes stable, cylindrical bridges, and for $\beta > \pi$, ● denotes the cylinder → amphora transition, ○ denotes pinch-off.

The agreement between the theory and experiment can be further improved by introducing the surface conductivity ratio as an adjustable parameter. Using the theory set out in § 5, surface conductivities needed to bring theory and experiment into agreement for the cylinder–amphora transitions were calculated, cf. table 1. While one expects the surface conductivities at the two aspect ratios to be closer to one another, it should be noted that only small amounts of electrolyte are needed to produce conductivities of this magnitude. Contamination may also be a factor. Another possibility is that the density of ions in the surface is field dependent. However, analysing these phenomena requires knowledge of electrokinetics in apolar liquids well beyond the scope of the current investigation.

β	$\Delta^{(1)}$	$\Delta^{(2)}$	$R_s^{(3)}$
3.23	0.26	0.031	3.33
4.32	0.64	0.283	0.59

(1) Field strength parameter measured by Burcham & Saville (2000)
(2) Field strength parameter predicted from the leaky dielectric model.
(3) Conductivity ratio required to bring theory and experiment into agreement.

TABLE 1. Experimental and theoretical cylinder amphora transition conditions for a castor oil bridge in SF_6 where $S = 0.215$.

7. Concluding remarks

Two points deserve final comment. First, the qualitative behaviour predicted by the Taylor–Melcher model accords with the experimental observations: namely, high field strengths stabilize an otherwise unstable configuration, the most unstable configuration is antisymmetric with respect to the midplane, and a bridge whose dielectric constant is lower than the surrounding fluid cannot be stabilized by a field. Second, although the quantitative agreement between theory and experiment for the cylinder–amphora transition is not as close as one might like, using surface transport as an adjustable parameter brings theory and experiment into agreement. However, this entails introducing a property that was not measured in the experimental study. Indeed, it is not clear how this measurement should be made. Nevertheless, the theory shows that bridge stability is acutely sensitive to surface transport. The field strength parameter measured at pinch-off compares favourably with the theoretical value from the linearized theory.

This work was supported by the National Aeronautics & Space Administration's Microgravity Science and Applications Division (NAG8-969). C. L. B. also received support from a NASA Graduate Student Research Fellowship and a DuPont Fellowship.

Appendix. Analysis of the antisymmetric modes

Following Nicolás (1992), the even P–F function,

$$\Psi_z(z) = \varphi_1^n(z), \tag{A 1}$$

is used for the z-dependence of the stream function for the antisymmetric solution. Joseph (1977) gives some convenient representations for the P–F functions:

$$\varphi_1^n(z) = \beta_n\beta \sin(\beta_n\beta)\cos(\beta_n z) - \beta_n z \cos(\beta_n\beta)\sin(\beta_n z), \tag{A 2}$$

$$\varphi_2^n(z) = -\varphi_1^n(z) - 2\cos(\beta_n\beta)\cos(\beta_n z). \tag{A 3}$$

Expression (A 3) will be useful when the pressure is computed. The r-dependence of the stream function found by separation of variables leads to an expression that satisfies the 'no-penetration' boundary condition on the electrodes,

$$\tilde{\psi}_i(r,z) = \omega r \sum_{n=-\infty}^{\infty} \frac{B_n}{\beta_n^2}\frac{I_1(\beta_n r)}{I_1(\beta_n)}\varphi_1^n(z). \tag{A 4}$$

To meet the 'no-slip' condition,

$$\varphi_1^{n'}(\pm\beta) = -\beta_n^2\beta - \beta_n \cos(\beta_n\beta)\sin(\beta_n\beta) = 0. \tag{A 5}$$

Hereafter prime symbols denote differentiation. Accordingly, we must have

$$\sin(2\beta_n\beta) + 2\beta_n\beta = 0, \tag{A 6}$$

which has complex roots. It follows that the arguments of the P–F functions and the coefficients in the stream function expansion are complex. The roots of the characteristic equation calculated here agree with the values published by Robbins & Smith (1948).

With the stream function in hand, the velocities and pressure can be calculated, i.e.

$$\tilde{u}(r,z) = -\omega \sum_{n=-\infty}^{\infty} \frac{B_n}{\beta_n^2} \frac{I_1(\beta_n r)}{I_1(\beta_n)} \varphi_1^{n'}(z), \tag{A 7}$$

$$\tilde{w}(r,z) = \omega \sum_{n=-\infty}^{\infty} \frac{B_n}{\beta_n} \frac{I_0(\beta_n r)}{I_1(\beta_n)} \varphi_1^{n}(z), \tag{A 8}$$

$$\tilde{p}_i(r,z) = -\omega \sum_{n=-\infty}^{\infty} \frac{B_n}{\beta_n} \frac{I_0(\beta_n r)}{I_1(\beta_n)} (\varphi_1^{n'}(z) + \varphi_2^{n'}(z)) + g_0, \tag{A 9}$$

with g_0 as a constant of integration. The remaining boundary conditions are used to find the unknown (complex) coefficients, B_n. Substituting the pressure, potential, and velocities into the normal stress condition produces a second-order non-homogeneous differential equation

$$\tilde{f}''(z) + \tilde{f}(z) = \omega \sum_{n=-\infty}^{\infty} \frac{B_n}{\beta_n} \left[\frac{I_0(\beta_n)}{I_1(\beta_n)} (\varphi_2^{n'}(z) - \varphi_1^{n'}(z)) + \frac{2}{\beta_n} \varphi_1^{n'}(z) \right] + \Delta(S-1) \sum_{\substack{k=1 \\ \text{odd}}}^{\infty} A_k \alpha_k \cos(\alpha_k(z+\beta)) - g_0. \tag{A 10}$$

The solution of this equation involves both P–F and Fourier series:

$$\tilde{f}(z) = b\sin(z) + c\cos(z) + \Delta(S-1) \sum_{\substack{k=1 \\ \text{odd}}}^{\infty} A_k \frac{\alpha_k}{1-\alpha_k^2} \cos(\alpha_k(z+\beta)) + \omega \sum_{n=-\infty}^{\infty} \frac{B_n}{\beta_n^2} [(C_n - 2D_n)\varphi_1^{n'}(z) - D_n \varphi_2^{n'}(z)] - g_0, \tag{A 11}$$

with

$$C_n = \frac{2 + r_n\beta_n(\beta_n^2 - 3)}{(1-\beta_n^2)^2}, \quad D_n = \frac{\beta_n(2\beta_n - r_n(1+\beta_n^2))}{(1-\beta_n^2)^2}, \tag{A 12}$$

and

$$r_n = \frac{I_0(\beta_n)}{I_1(\beta_n)}. \tag{A 13}$$

Next, we impose the requirements of conservation of volume

$$c\sin(\beta) - g_0\beta = 0 \tag{A 14}$$

and pinning of contact lines at the two electrodes,

$$b\sin(\beta)+c\cos(\beta)-g_0-\Delta(S-1)\sum_{\substack{k=1\\ \text{odd}}}^{\infty}A_k\frac{\alpha_k}{1-\alpha_k^2}+2\beta\omega\sum_{m=-\infty}^{\infty}B_mD_m=0, \tag{A 15}$$

$$-b\sin(\beta)+c\cos(\beta)-g_0+\Delta(S-1)\sum_{\substack{k=1\\ \text{odd}}}^{\infty}A_k\frac{\alpha_k}{1-\alpha_k^2}-2\beta\omega\sum_{m=-\infty}^{\infty}B_mD_m=0. \tag{A 16}$$

From these expressions it follows that $c=g_0=0$. Conservation of charge across the interface gives

$$\begin{aligned}\sum_{\substack{k=1\\ \text{odd}}}^{\infty}A_k\left(\frac{\alpha_kI_1(\alpha_k)}{I_0(\alpha_k)}+R\frac{\alpha_kK_1(\alpha_k)}{K_0(\alpha_k)}-\Delta(S-1)(R-1)\frac{\alpha_k^2}{1-\alpha_k^2}\right)\sin(\alpha_k(z+\beta))&\\ +\omega(R-1)\sum_{m=-\infty}^{\infty}B_m(D_m\varphi_1^m(z)+C_m\varphi_2^m(z))&\\ +(R-1)b\cos(z)-(R-1)c\sin(z)=0.&\end{aligned} \tag{A 17}$$

From the orthogonal properties of the Fourier series

$$\int_{-\beta}^{\beta}\sin(\alpha_1(z+\beta))\sin(\alpha_k(z+\beta))\,\mathrm{d}z=\beta\delta_{lk} \tag{A 18}$$

where δ_{lk} is the Kronecker delta. Applying the integral operator

$$\int_{-\beta}^{\beta}\sin(\alpha_1(z+\beta))(\cdot)\,\mathrm{d}z \tag{A 19}$$

to (A 17) gives

$$(R-1)Z_lb+A_kS_k\beta\delta_{lk}+\omega(R-1)\sum_{m=-\infty}^{\infty}B_mD_mP_{lm}+\omega(R-1)\sum_{m=-\infty}^{\infty}B_mC_mQ_{lm}=0 \tag{A 20}$$

with (note: l is an odd integer)

$$S_k=\frac{\alpha_kI_1(\alpha_k)}{I_0(\alpha_k)}+R\frac{\alpha_kK_1(\alpha_k)}{K_0(\alpha_k)}-\Delta(S-1)(R-1)\frac{\alpha_k^2}{1-\alpha_k^2}, \tag{A 21}$$

$$P_{lm}=\int_{-\beta}^{\beta}\varphi_1^m(z)\sin(\alpha_l(z+\beta))\,\mathrm{d}z=4\alpha_l\frac{\beta_m^2\cos^2(\beta\beta_m)}{(\alpha_l^2-\beta_m^2)^2}, \tag{A 22}$$

$$Q_{lm}=\int_{-\beta}^{\beta}\varphi_2^m(z)\sin(\alpha_l(z+\beta))\,\mathrm{d}z=-4\alpha_l^3\frac{\cos^2(\beta\beta_m)}{(\alpha_l^2-\beta_m^2)^2}, \tag{A 23}$$

$$Z_l=\int_{-\beta}^{\beta}\sin(\alpha_l(z+\beta))\cos(z)\,\mathrm{d}z=-2\alpha_l\frac{\cos(\beta)}{1-\alpha_l^2}. \tag{A 24}$$

Equation (A 20) becomes

$$(R-1)Z_lb+A_lS_l\beta+\omega(R-1)\sum_{m=-\infty}^{\infty}B_mD_mP_{lm}+\omega(R-1)\sum_{m=-\infty}^{\infty}B_mC_mQ_{lm}=0. \tag{A 25}$$

The kinematic condition gives

$$\tilde{f}(z) = -\sum_{n=-\infty}^{\infty} \frac{B_n}{\beta_n^2} \varphi_1^{n'}(z). \tag{A 26}$$

Next these expressions are combined with (A 11) and the derivative of the resultant expression used to write an equation in terms of $\varphi_1^n(z)$ and $\varphi_2^n(z)$, exploiting the properties of the Papkovich–Fadle functions. From the properties of P–F functions it follows that

$$\frac{1}{\beta_m^2}(C_m - 2D_m)\varphi_1^{m''}(z) - D_m\varphi_2^{m''}(z) = D_m\varphi_1^m(z) + C_m\varphi_2^m(z) \tag{A 27}$$

so

$$b\cos(z) - \sum_{\substack{k=1 \\ \text{odd}}}^{\infty} A_k U_k \sin(\alpha_k(z+\beta)) + \sum_{m=-\infty}^{\infty} B_m\varphi_2^m(z) + \omega \sum_{m=-\infty}^{\infty} B_m(D_m\varphi_1^m(z) + C_m\varphi_2^m(z)) = 0 \tag{A 28}$$

with

$$U_k = \Delta(S-1)\frac{\alpha_k^2}{1-\alpha_k^2}. \tag{A 29}$$

Finally, the velocity, pressure, electric field and derivative of $\tilde{f}(z)$ with respect to z are substituted into the tangential stress condition, giving

$$\Delta(S-1)\cos(z)b + \sum_{\substack{k=1 \\ \text{odd}}}^{\infty} A_k T_k \sin(\alpha_k(z+\beta))$$
$$+\omega \sum_{m=-\infty}^{\infty} B_m((1 + D_m\Delta(S-1))\varphi_1^m(z) + (-1 + C_m\Delta(S-1))\varphi_2^m(z)) = 0, \tag{A 30}$$

with

$$T_k = \Delta\alpha_k \left[\frac{I_1(\alpha_k)}{I_0(\alpha_k)} + S\frac{K_1(\alpha_k)}{K_0(\alpha_k)} - \Delta(S-1)^2\frac{\alpha_k}{1-\alpha_k^2}\right]. \tag{A 31}$$

Equations (A28) and (A30) can be written in matrix form:

$$\begin{bmatrix} -\Delta(S-1) \\ -1 \end{bmatrix} b\cos(z) = \sum_{\substack{k=1 \\ \text{odd}}}^{\infty} A_k \sin(\alpha_k(z+\beta)) \begin{bmatrix} T_k \\ -U_k \end{bmatrix} + \sum_{m=-\infty}^{\infty} B_m \begin{bmatrix} 1 & 0 \\ 0 & 1 \end{bmatrix} \begin{bmatrix} \varphi_1^m(z) \\ \varphi_2^m(z) \end{bmatrix}$$
$$+ \sum_{m=-\infty}^{\infty} B_m \begin{bmatrix} -1 + \omega(1 + D_m\Delta(S-1)) & \omega(-1 + C_m\Delta(S-1)) \\ \omega D_m & \omega C_m \end{bmatrix} \begin{bmatrix} \varphi_1^m(z) \\ \varphi_2^m(z) \end{bmatrix}. \tag{A 32}$$

The biorthogonal condition for the P–F functions is

$$\int_{-\beta}^{\beta} [\psi_1^n(z)\psi_2^n(z)] \begin{bmatrix} 0 & -1 \\ 1 & 2 \end{bmatrix} \begin{bmatrix} \varphi_1^m(z) \\ \varphi_2^m(z) \end{bmatrix} \mathrm{d}z = j_m\delta_{nm}, \tag{A 33}$$

where $\psi_1^n(z)$ and $\psi_2^n(z)$ are the adjoint eigenfunctions given by (Joseph 1977)

$$\psi_l^n(z) = \varphi_1^n(z) - 2\cos(\beta_n\beta)\cos(\beta_n z), \psi_2^n(z) = \varphi_1^n(z), \quad j_m = -4\beta\cos^4(\beta_m\beta). \tag{A 34}$$

So, applying the operator

$$\int_{-\beta}^{\beta} [\psi_1^n(z)\psi_2^n(z)] \begin{bmatrix} 0 & -1 \\ 1 & 2 \end{bmatrix} \begin{bmatrix} \cdot \\ \cdot \end{bmatrix} \mathrm{d}z \tag{A 35}$$

to (A 32) gives

$$\begin{aligned} 0 = {} & (-X_n + 2Y_n)b + B_n J_n + \omega \sum_{m=-\infty}^{\infty} B_m[(-I_{nm} + 2J_{nm})D_m + (-L_{nm} + 2K_{nm})C_m] \\ & + \Delta(S-1)Y_n b + \sum_{\substack{k=1 \\ \text{odd}}}^{\infty} A_k(U_k M_{nk} + (T_k - 2U_k)N_{nk}) \\ & + \Delta(S-1)\omega \sum_{m=-\infty}^{\infty} B_m[D_m J_{nm} + C_m K_{nm}] + \omega \sum_{m=-\infty}^{\infty} B_m[J_{nm} - K_{nm}] - \sum_{m=-\infty}^{\infty} B_m J_{nm} \end{aligned} \tag{A 36}$$

with the following definitions:

$$\begin{aligned} I_{nm} &= \int_{-\beta}^{\beta} \psi_1^n(z)\varphi_1^m(z)\,\mathrm{d}z \\ &= \begin{cases} -8\beta\beta_m^2(\beta_m^2 - 3\beta_n^2)\dfrac{(\beta_m^2\cos^2(\beta\beta_n) - \beta_n^2\cos^2(\beta\beta_m))}{(\beta_m^2 - \beta_n^2)^3}, & n \neq m \\ 3\beta^3\beta_n^2 - \beta\cos^2(\beta\beta_n)(3 + \frac{2}{3}\beta^2\beta_n^2), & n = m, \end{cases} \end{aligned} \tag{A 37}$$

$$J_{nm} = \int_{-\beta}^{\beta} \psi_2^n(z)\varphi_1^m(z)\,\mathrm{d}z = \begin{cases} 16\beta\beta_m^2\beta_n^2\dfrac{(\beta_m^2\cos^2(\beta\beta_n) - \beta_n^2\cos^2(\beta\beta_m))}{(\beta_m^2 - \beta_n^2)^3}, & n \neq m \\ \beta^3\beta_n^2 - \beta\cos^2(\beta\beta_n)(1 + \frac{2}{3}\beta^2\beta_n^2), & n = m, \end{cases} \tag{A 38}$$

$$\begin{aligned} K_{nm} &= \int_{-\beta}^{\beta} \psi_2^n(z)\varphi_2^m(z)\,\mathrm{d}z \\ &= \begin{cases} -8\beta\beta_n^2(\beta_m^2 + \beta_n^2)\dfrac{(\beta_m^2\cos^2(\beta\beta_n) - \beta_n^2\cos^2(\beta\beta_m))}{(\beta_m^2 - \beta_n^2)^3}, & n \neq m \\ \beta^3\beta_n^2 - \beta\cos^2(\beta\beta_n)(1 - \frac{2}{3}\beta^2\beta_n^2), & n = m, \end{cases} \end{aligned} \tag{A 39}$$

$$L_{nm} = \int_{-\beta}^{\beta} \psi_1^n(z)\varphi_2^m(z)\,\mathrm{d}z = \begin{cases} -16\beta\beta_n^4\dfrac{(\beta_m^2\cos^2(\beta\beta_n) - \beta_n^2\cos^2(\beta\beta_m))}{(\beta_m^2 - \beta_n^2)^3}, & n \neq m \\ -\beta^3\beta_n^2 + \beta\cos^2(\beta\beta_n)(1 + \frac{2}{3}\beta^2\beta_n^2), & n = m, \end{cases} \tag{A 40}$$

$$M_{nk} = \int_{-\beta}^{\beta} \psi_1^n(z)\sin(\alpha_k(z+\beta))\,\mathrm{d}z = -4\alpha_k\frac{\cos^2(\beta\beta_n)(\alpha_k^2 - 2\beta_n^2)}{(\alpha_k^2 - \beta_n^2)^2}, \tag{A 41}$$

$$N_{nk} = \int_{-\beta}^{\beta} \psi_2^n(z)\sin(\alpha_k(z+\beta))\,\mathrm{d}z = 4\alpha_k\frac{\beta_n^2\cos^2(\beta\beta_n)}{(\alpha_k^2 - \beta_n^2)^2}, \tag{A 42}$$

$$X_n = \int_{-\beta}^{\beta} \psi_1^n(z)\cos(z)\,\mathrm{d}z = -4\frac{(1-2\beta_n^2)}{(1-\beta_n^2)^2}(\cos^2(\beta_n\beta)\sin(\beta) + \beta\beta_n^2\cos(\beta)), \tag{A 43}$$

$$Y_n = \int_{-\beta}^{\beta} \psi_2^n(z)\cos(z)\,\mathrm{d}z = 4\frac{\beta_n^2}{(1-\beta_n^2)^2}(\cos^2(\beta\beta_n)\sin(\beta) + \beta\beta_n^2\cos(\beta)). \tag{A 44}$$

There are $(L+1)/2$ (real) A_k, $2N$ (complex) B_k and one (real) b. Written symbolically in matrix form

$$\begin{bmatrix} \{\text{Equation (A 36)}\} \\ \{\text{Equation (A 25)}\} \\ \{\text{Equation (A 15)}\} \end{bmatrix} \begin{bmatrix} B_m \\ A_k \\ b \end{bmatrix} = \begin{bmatrix} 0 \\ 0 \\ 0 \end{bmatrix}. \tag{A 45}$$

Since the determinant of the matrix in this equation must be zero, the computation is reduced to an eigenvalue problem for ω, given R, S, β, and Δ. At the neutral stability point, ω vanishes. The solution for symmetric deformations proceeds in a similar fashion (Burcham 1998).

REFERENCES

Allan, R. S. & Mason, S. G. 1962 Particle behaviour in shear and electric fields. I. Deformation and burst of fluid drops. *Proc. R. Soc. Lond.* A, **267**, 45–61.

Burcham, C. L. 1998 The electrohydrodynamic stability of a leaky dielectric liquid bridge in an axial electric field with zero Bond number. PhD thesis, Princeton University.

Burcham, C. L. & Saville, D. A. 2000 The electrohydrodynamic stability of a liquid bridge: microgravity experiments on a bridge suspended in a dielectric gas. *J. Fluid Mech.* **405**, 37–56.

Feng, J. Q. 1999 Electrohydrodynamic behaviour of a drop subjected to a steady uniform electric field at finite electric Reynolds number. *Proc. R. Soc. Lond.* A **445**, 2245–2269.

Feng, J. Q. & Scott, T. C. 1996 A computational analysis of electrohydrodynamics of a leaky dielectric drop in an electric field. *J. Fluid Mech.* **311**, 289–326.

González, H. & Castellanos, A. 1993 The effect of residual gravity on the stability of liquid columns subjected to electric fields. *J. Fluid Mech.* **249**, 185–206.

González, H., McCluskey, F. M. J., Castellanos, A. & Barrero, A. 1989 Stabilization of dielectric liquid bridges by electric fields in the absence of gravity. *J. Fluid Mech.* **206**, 545–561.

Joseph, D. D. 1975 Slow motion and viscometric motion; stability and bifurcation of the rest state of a simple fluid. *Arch. Rat. Mech. Anal.* **56**, 99–157.

Joseph, D. D. 1977 The convergence of biorthogonal series for biharmonic and Stokes flow edge problems: Part I. *SIAM J. Appl. Maths* **33**, 337–347.

Joseph, D. D. & Sturges, L. 1975 The free surface on a liquid filling a trench heated from its side. *J. Fluid Mech.* **69**, 565–589.

Joseph, D. D. & Sturges. L. 1978 The convergence of biorthogonal series for biharmonic and Stokes flow edge Problems: Part II. *SIAM J. Appl. Maths* **34**, 7–26.

Melcher, J. R. & Taylor, G. I. 1969 Electrohydrodynamics: a review of the role of interfacial shear stresses. *Annu. Rev. Fluid Mech.* **1**, 111–147.

Nayyar, N. K. & Murty, G. S. 1960 The stability of a dielectric liquid jet in the presence of a longitudinal electric field. *Proc. Phys. Soc.* **75**, 369–373.

Nicolás, J. A. 1992 Hydrodynamic stability of high viscosity cylindrical liquid bridges. *Phys. Fluids* **4**, 1620–1626.

Plateau, J. 1863 Experimental and theoretical researches on the figures of equilibrium of a liquid mass withdrawn from the action of gravity, etc. *Annual Report of the Board of Regents of the Smithsonian Institution, Pt. 1, House of Representatives Misc. Doc. #83, 38th Congress, 1st Session*, pp. 207–285.

Plateau, J. 1864 Experimental and theoretical researches on the figures of equilibrium of a liquid mass withdrawn from the action of gravity, etc. *Annual Report of the Board of Regents of the Smithsonian Institution, Pts. 2–4, House of Representatives Misc. Doc. #54, 38th Congress, 2nd Session*, pp. 285–369.

Plateau. J. 1865 Experimental and theoretical researches on the figures of equilibrium of a liquid

mass withdrawn from the action of gravity, etc. *Annual Report of the Board of Regents of the Smithsonian Institution, Pt. 5, House of Representatives Misc. Doc.* #102, *39th Congress, 2nd Session*, pp. 411–435.

Plateau, J. 1866 Experimental and theoretical researches on the figures of equilibrium of a liquid mass withdrawn from the action of gravity, etc. *Annual Report of the Board of Regents of the Smithsonian Institution, Pt. 6, House of Representatives Misc. Doc.* #83, *39th Congress, 2nd Session*, pp. 255–289.

Raco, R. J. 1968 Electrically supported column of liquid. *Science* **160**, 311–312.

Ramos, A., González, H. & Castellanos, A. 1994 Experiments on dielectric liquid bridges subjected to axial electric fields. *Phys. Fluids* **6**, 3206–3208.

Rayleigh, Lord 1878 On the instabilities of jets. *Proc. Lond. Math. Soc.* **10**, 4–13.

Rayleigh, Lord 1879*a* The influence of electricity on colliding water drops. *Proc. R. Soc.* **28**, 406–409.

Rayleigh, Lord 1879*b* On the capillary phenomena of jets. *Proc. R. Soc.* **29**, 71–97.

Rayleigh, Lord 1882 On the equilibrium of liquid conducting masses charged with electricity. *Phil. Mag.* (5) **14**, 184–186.

Rayleigh, Lord 1891 Some applications of photography. *Nature* **44**, 249–254.

Rayleigh, Lord 1892 On the instability of a cylinder of viscous liquid under capillary forces. *Phil. Mag.* (5) **34**, 207, 145.

Robbins, C. I. & Smith, R. C. T. 1948 A table of roots of Sin $Z = -Z$. *Phil. Mag.* **39**, 1004–1005.

Russel, W. B., Saville, D. A. & Schowalter, W. R. 1991 *Colloidal Dispersions.* Cambridge University Press.

Sankaran, S. & Saville, D. A. 1993 Experiments on the stability of a liquid bridge in an axial electric field. *Phys. Fluids* **5**, 1081–1083.

Saville, D. A. 1970 Electrohydrodynamic stability: fluid cylinders in longitudinal electric fields. *Phys. Fluids* **13**, 2987–2994.

Saville, D. A. 1971 Stability of electrically charged viscous cylinders. *Phys. Fluids* **14**, 1095–1099.

Saville, D. A. 1997 Electrohydrodynamics: the Taylor-Melcher leaky dielectric model. *Annu, Rev. Fluid Mech.* **29**, 27–64.

Smith, R. C. T. 1952 The Bending of a Semi-Infinite Strip. *Austral. J. Sci. Res.* A *Phys. Sci.* **5**, 227–237.

Taylor, G. I. 1966 Studies in electrohydrodynamics. I. The circulation produced in a drop by an electric field. *Proc. R. Soc. Lond.* A **291**, 159–166.

Taylor, G. I. 1969 Electrically driven jets. *Proc. R. Soc. Lond.* A **313**, 453–475.

Torza, S., Cox, R. G. & Mason, S. G. 1971 Electrodydrodynamic deformation and burst of Liquid drops. *Phil. Trans. R. Soc. Lond.* A **269**, 295–319.

Tsukada, T., Katayama, T., Ito, Y. & Mitsunori, H. 1993 Theoretical and experimental studies of circulations inside and outside a deformed drop under a uniform field. *J. Chem. Engng Japan* **26**, 698–703.

Vizika, O. & Saville, D. A. 1992 The electrohydrodynamic deformation of drops suspended in liquids in steady and oscillatory fields. *J. Fluid Mech.* **239**, 1–16.